Snaking and isolas of localised states in bistable discrete lattices

Chris Taylor[a,1], Jonathan H.P. Dawes[b,2]

[a] *Department of Applied Mathematics and Theoretical Physics, Centre for Mathematical Sciences, University of Cambridge, Wilberforce Road, Cambridge CB3 0WA, UK*
[b] *Department of Mathematical Sciences, University of Bath, Claverton Down, Bath BA2 7AY, UK*

Abstract

We consider localised states in a discrete bistable Allen-Cahn equation. This model equation combines bistability and local cell-to-cell coupling in the simplest possible way. The existence of stable localised states is made possible by pinning to the underlying lattice; they do not exist in the equivalent continuum equation.

In particular we address the existence of 'isolas': closed curves of solutions in the bifurcation diagram. Isolas appear for some non-periodic boundary conditions in one spatial dimension but seem to appear generically in two dimensions. We point out how features of the bifurcation diagram in 1D help to explain some (unintuitive) features of the bifurcation diagram in 2D.

Key words: homoclinic snaking, dissipative soliton, coupled cells
PACS: 0545.-a, 42.65.Sf

1. Introduction

The general term 'pattern formation' refers to the spontaneous appearance of structure in a dissipative dynamical system in a continuum or spatially discrete medium, when a spatially homogeneous state undergoes an instability of some kind [12, 16, 21]. In many physical situations it is appropriate to use mathematical models for which the spatial dynamics are modelled discretely, rather than as a continuum. Such lattice models arise in many physical applications: in particular we mention recent work in nonlinear optics [26, 27, 8] and mathematical modelling of processes in developmental biology [10, 20, 24]. In many applications the existence of domain-filling (almost) regular solutions exhibiting spatial periodicity is of interest. Mathematical work on periodic patterns in regular lattices has also been the subject of considerable recent interest [23, 2].

In addition, there has been a renewed interest in the study of localised states in nonlinear dissipative systems in recent years, motivated by a wealth of experimental and numerical results both in continuum systems [11, 4, 5] and spatially discrete models [1]. Such localised states have been referred to by a number of different names, including 'light bullets' and 'dissipative solitons'.

In continuum systems one recurring mechanism for the generation of localised states is the existence of a subcritical Turing (pattern-forming) instability. In the simplest case, two branches of small-amplitude localised states emerge at the Turing instability, also in this context referred to as a Hamiltonian–Hopf bifurcation [17]. Away from the initial instability they develop into a complicated structure of fully nonlinear localised states which exist on a pair of intertwining curves [25]; a complete asymptotic description of the bifurcation structure involves consideration of exponentially-small effects [18, 7]. In an infinite domain this 'homoclinic snaking' behaviour continues, and the width of the localised states increases without bound. In a finite domain the branches of localised states terminate on the branches of spatially periodic patterns which also originate at the initial Turing instability [3, 13]. There is now a pretty complete picture of the

[1] CRNT acknowledges financial support from the EPSRC.
[2] JHPD holds a University Research Fellowship from the Royal Society.

existence and stability of localised states in canonical 1D model equations, for example the Swift–Hohenberg model [22] with quadratic-cubic or cubic-quintic nonlinearities, but in contrast, comparatively little is known about the detailed structure of localised states in spatially discrete problems.

Motivation for the detailed investigation of discrete models comes from a number of sources, but in particular discrete models arise as natural descriptions of arrays of waveguides in nonlinear optics [26]. For example, the discrete bistable nonlinear Schrödinger equation

$$\mathrm{i}\dot{\psi}_n + C\Delta\psi_n + s\psi_n|\psi_n|^2 - \psi_n|\psi_n|^4 = 0, \tag{1}$$

for an array of complex fields $\psi_n(t)$ naturally describes properties of discrete optical 'dissipative solitons' in a k-dimensional square lattice whose sites are indexed by the (multiple) suffix $n \in \mathbb{Z}^k$. The operator Δ is an appropriate sum of nearest neighbour (and possibly next-nearest neighbour) differences depending on the lattice dimension k. Substituting the ansatz $\psi_n = u_n \exp(-\mathrm{i}\mu t)$ where u_n is a real stationary field, we see that u_n must satisfy the real difference equation

$$\mu u_n + C\Delta u_n + s u_n^3 - u_n^5 = 0. \tag{2}$$

Hence the possible steady states correspond to those of a discrete Allen–Cahn equation [9], albeit with a cubic-quintic nonlinearity rather than the well-studied purely cubic case.

In this Letter we investigate the existence of localised states in the canonical nonlinear lattice model (2) in one and two dimensions. Such models are in many senses simpler than the corresponding spatially continuous equations and we discuss the similarities and differences that arise. To aid this discussion we add a time derivative term to (2) which makes stability correspond to that found in the spatially-continuous Swift–Hohenberg model. In contrast to previous work on this canonical problem by other authors, our central focus in this paper is on the appearance of isolas. In particular we show that, firstly, in 1D and on a finite lattice, isolas are an immediate consequence of changing the boundary conditions from periodic to Neumann (or, in fact Dirichlet). Secondly we show that in 2D isolas exist when periodic boundary conditions are used, and reconnect and then disconnect again as the cell to cell coupling parameter is increased. We also comment on (i) the overall bifurcation structure in 1D, (ii) the similarities between the 1D bifurcation structure and that of the continuum 1D Swift–Hohenberg model and (iii) the connections between 1D lattice structures and 2D lattice structures, using the former to explain features of the bifurcation diagram we obtain for the latter.

The structure of the Letter is as follows. In section 2 we introduce the 1D lattice case and explore the bifurcation structure of localised states. We discuss the effects of different boundary conditions when the problem is restricted to a finite lattice. In section 3 we consider a 2D lattice, highlight the new features that arise, and use the 1D results to explain aspects of the snaking curve. We summarise the main results of the paper in section 4.

2. One-dimensional lattices

Motivated by (2), after applying the rescaling $u_n = \sqrt{\frac{s}{2}}\tilde{u}_n$, rescaling μ and C appropriately, dropping the tilde and adding a time derivative term appropriate for strongly dissipative rather than conservative dynamics, we consider the following equation posed on the integer lattice $\mathbb{Z}$:

$$\dot{u}_n = C(u_{n+1} + u_{n-1} - 2u_n) + \mu u_n + 2u_n^3 - u_n^5, \tag{3}$$

where u_n is a real scalar variable defined at each lattice site, C is the strength of linear coupling between adjacent sites, and $-1 < \mu < 0$ is the primary (real) bifurcation parameter. The addition of a time derivative term is, of course, not necessary for the investigation of the existence of equilibrium states. However, it is a useful addition to indicate stability and to provide a contextual similarity to the studies of the Swift–Hohenberg equation in spatially continuous systems referred to above. If $C < 0$ then we apply the parameter symmetry given by applying the 'staggering' transformation

$$u_n \to (-1)^n u_n, \quad C \to -C, \quad \mu \to \mu - 4C, \tag{4}$$

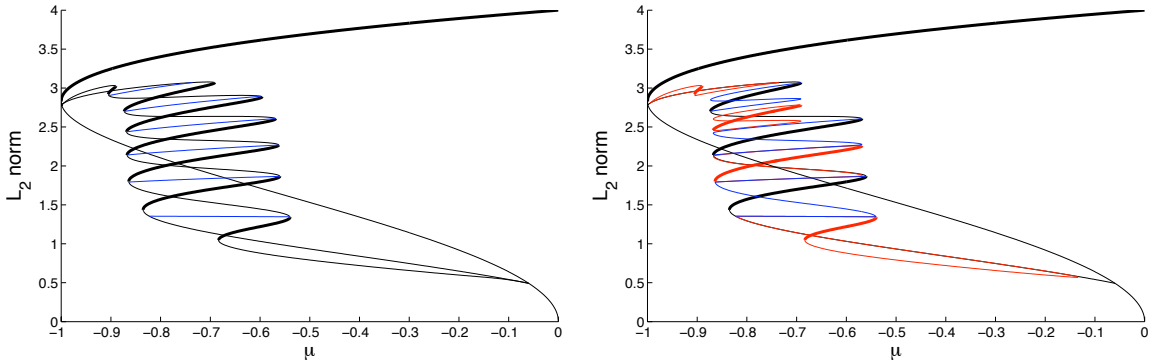

(a) (b)

Figure 1: (a) Bifurcation diagram in one dimension for an array of $N = 8$ cells with PBC and coupling strength $C = 0.2$. Thick lines represent stable solutions, thin lines represent unstable solutions. The thin blue horizontal lines are asymmetric 'ladder' solutions. (b) The bifurcation diagram with NBC. Red curves are isolas, and blue curves terminate at branch points on the black snaking curve. The red isolas and blue bubbles appear alternately: four red isolas are shown; both the lowest and the highest parts of the snaking curve form isolas in this case. Three blue bubbles are shown as thin lines between the isolas.

which leaves the equation unchanged, but switches the sign of C. Thus in this Letter we will only consider positive C, noting that the existence (and stability) of states $\{u_n\}$ with $C > 0$ is equivalent to the existence (and stability) of states $\{v_n\} = \{(-1)^n u_n\}$ when $C < 0$ and μ is shifted as in (4).

Importantly, and in common with the Swift–Hohenberg equation, equation (3) is a gradient flow, that is, we can write $\dot{u}_n = -\partial F/\partial u_n$ where the potential F is given by

$$F(u) = \sum_n \tfrac{1}{2}C(u_{n+1} - u_n)^2 - \tfrac{1}{2}\mu u_n^2 - \tfrac{1}{2}u_n^4 + \tfrac{1}{6}u_n^6. \tag{5}$$

Thus $\dot{F} \leq 0$, so that every solution of (3) flows down gradients of the potential toward an equilibrium solution, and every stable equilibrium state is a local minimum of the potential. No periodic or complex dynamics are therefore possible.

There are five homogeneous equilibria: the trivial state $u_n = 0$, and four non-trivial equilibria $u_n = \pm u_\pm$, where

$$u_\pm^2 = 1 \pm \sqrt{1+\mu}. \tag{6}$$

The state $u_n = 0$ is linearly stable for $\mu < 0$ and unstable for $\mu > 0$. Taking the positive square roots, the lower uniform state $u_- = \sqrt{1 - \sqrt{1+\mu}}$ exists in $-1 < \mu < 0$ and is always unstable, and the upper uniform state $u_+ = \sqrt{1 + \sqrt{1+\mu}}$ exists in $\mu > -1$ and is always stable; there is a saddle-node bifurcation at $\mu = -1$.

The per-cell potential for a homogeneous equilibrium $u_n = u_*$ is given by $F(u_*) = -\frac{1}{2}\mu u_*^2 - \frac{1}{4}u_*^4 + \frac{1}{6}u_*^6$. Since the system acts to minimize the total potential, the relative values of potential at the homogeneous equilibria are important. The zero state has zero potential, and the potential of the upper state u_+ depends only on μ. By looking for a double root of $F(u) = 0$ we find that the upper state has zero potential when $\mu = \mu_{\rm mx} = -3/4$; this is the so-called *Maxwell point* at which the upper uniform state and the zero state are energetically equal. When $\mu > \mu_{\rm mx}$ the upper state is energetically more favourable; when $\mu < \mu_{\rm mx}$ the zero state is energetically more favourable.

2.1. Boundary conditions

In many physical applications it is appropriate to consider (3) posed on a finite grid $n \in \{1, \ldots, N\}$ with boundary conditions specified with the aid of 'ghost cells' u_0 and u_{N+1}. There are three obvious choices: periodic boundary conditions (PBC) for which $u_0 = u_N$ and $u_{N+1} = u_1$, Neumann boundary

conditions (NBC) for which $u_0 = u_1$ and $u_{N+1} = u_N$, and Dirichlet boundary conditions (DBC) for which $u_0 = u_{N+1} = 0$.

With PBC or NBC the homogeneous state is an equilibrium configuration. With DBC this is not the case and this obvious difference leads us to focus in this discussion only on PBC and NBC: we find there are substantial differences between these two cases that require some discussion.

2.2. Symmetries

Equation (3) posed on the infinite integer lattice has a symmetry group generated by the independent operations of translation τ, reflection ρ and an up-down symmetry κ (since the nonlinearity is an odd function of u_n):

$$\tau : u_n \mapsto u_{n+1}, \quad \rho : u_n \mapsto u_{-n}, \quad \kappa : u_n \mapsto -u_n. \tag{7}$$

Thus the full symmetry group of the infinite lattice problem is $\mathbb{Z} \ltimes \mathbb{Z}_2 \times \mathbb{Z}_2$. Posing the equation on a finite lattice implies changes in the symmetry group. Consider the following actions of the elements τ, ρ and κ:

$$\tau : u_n \mapsto u_{n+1\,(\mathrm{mod}N)}, \quad \rho : u_n \mapsto u_{N+1-n}, \quad \kappa : u_n \mapsto -u_n. \tag{8}$$

With PBC the translation subgroup $\mathbb{Z}$, generated by τ, is simply replaced with the cyclic group $\mathbb{Z}_N$ so that the full symmetry group is $\mathbb{Z}_N \ltimes \mathbb{Z}_2 \times \mathbb{Z}_2 \cong D_N \times \mathbb{Z}_2$. With NBC or DBC we lose translation symmetry entirely, so the symmetry group becomes $\mathbb{Z}_2 \times \mathbb{Z}_2 = \langle\rho\rangle \times \langle\kappa\rangle$.

We will be particularly interested in localised solutions to (3) which lie in $\mathrm{Fix}(\rho)$ or $\mathrm{Fix}(\rho\tau)$, i.e. which are symmetric under reflection either about a lattice point, or about a point halfway between two lattice points. We refer to such solutions as *site-centred* and *bond-centred*. When N is even, site-centred solutions lie in $\mathrm{Fix}(\rho\tau)$ and bond-centred solutions lie in $\mathrm{Fix}(\rho)$. When N is odd, site-centred solutions lie in $\mathrm{Fix}(\rho)$ and bond-centred solutions lie in $\mathrm{Fix}(\rho\tau)$.

2.3. Linear stability on a finite lattice

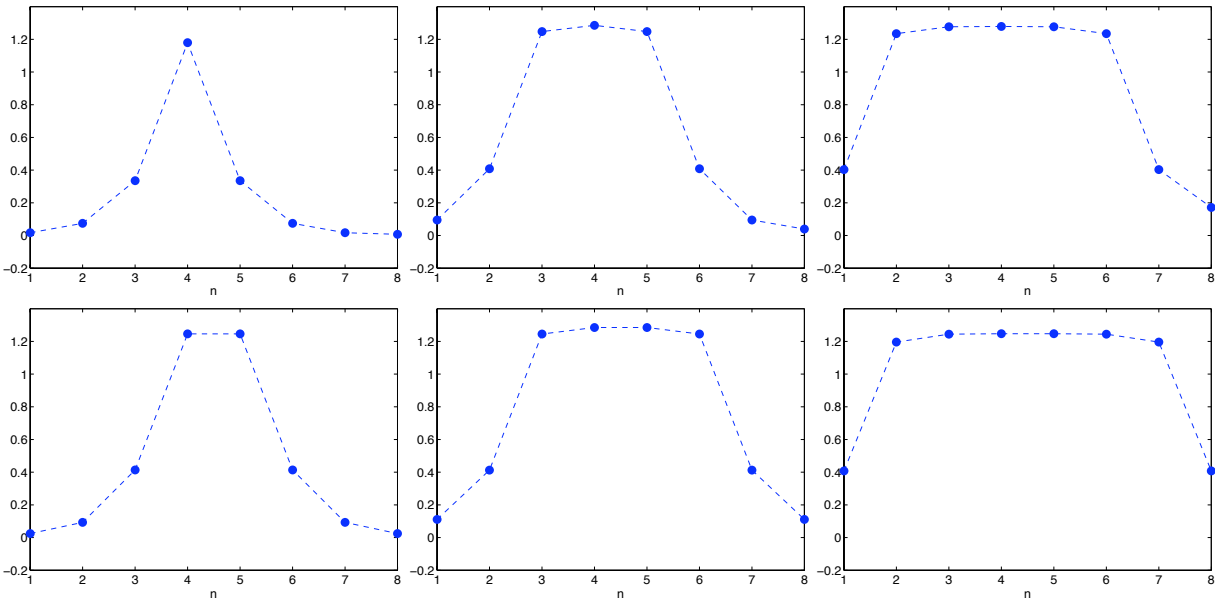

Figure 2: Equilibrium solution profiles of (3) solved on a 1D lattice with $N = 8$ using PBC and taking $C = 0.2$. Profiles correspond to the right-hand saddle-node bifurcation points of Figure 1(a). The upper three solutions are site-centered and hence are reflection-symmetric about the lattice point $n = 4$, since N is even in this case. Similarly, the lower three plots are bond-centred and are reflection-symmetric about the midpoint of sites $n = 4$ and $n = 5$.

The eigenfunctions $v_n^{(k)}$ and eigenvalues λ_k of the discrete Laplacian, obtained by solving $\Delta v_n^{(k)} \equiv v_{n+1}^{(k)} - 2v_n^{(k)} + v_{n-1}^{(k)} = \lambda v_n^{(k)}$ on an N-cell lattice with PBC are easily computed to be $v_n^{(k)} = \mathrm{e}^{\mathrm{i}\theta_k n}$ and $\lambda_k = -4\sin^2(\theta_k/2)$ where $\theta_k = 2\pi k/N$ for $k = 0, \ldots, N-1$. Thus the zero state undergoes an instability to a mode with 'wavenumber' parameter θ_k when $\mu = 4C\sin^2(\theta_k/2)$. Since $C > 0$ the first instability encountered when increasing μ is a bifurcation to the lower uniform state u_- at $\mu = 0$. This branch bifurcates subcritically, turning around in a saddle-node bifurcation and restabilising at $\mu = -1$ to form the upper uniform state u_+ as shown in figure 1.

The upper uniform state u_+ undergoes no instabilities as μ is increased. In contrast, the lower state u_- has many secondary bifurcation points, occuring at

$$\mu = \mu_k^{\pm} \stackrel{\text{def}}{=} -\tfrac{1}{2} - C\sin^2(\theta_k/2) \pm \sqrt{\tfrac{1}{4} - C\sin^2(\theta_k/2)}, \tag{9}$$

for values of k such that the expression under the square root is positive. The bifurcations are supercritical 'double pitchforks', each creating two new bifurcating branches of 'odd' and 'even' modulated states which develop into single- and multi-pulse localised states, each of which terminates on u_- at both ends. In figure 1 only the single pulse branches are shown for clarity. This behaviour of secondary bifurcation creating branches of odd and even-symmetric modulated and localised states is extremely similar to that given for the continuum Swift–Hohenberg equation in [3, 13] without the additional complexity that arises from continuous changes of wavenumber along the branch which is prohibited in the present case by the spatial discreteness.

Noting that the instability creating single-pulse localised states is the $k = 1$ branch, inspection of (9) shows that the $k = 1$ case is the last instability to remain as C increases at fixed N. Hence the maximum coupling strength above which there are no modulational instabilities of u_- is $C_{\max} = 1/[4\sin^2(\pi/N)]$. $C_{\max}$ therefore also provides an upper bound on the range of C over which localised states asymptotic to zero may exist.

2.4. Homoclinic snaking

We use the numerical continuation program AUTO [14] to explore the bifurcation structure of localised solutions to (3) using both PBC and NBC. Stability results come directly from AUTO, since (3) is simply a collection of ODEs.

With PBC the bifurcation diagram figure (1) closely resembles the homoclinic snaking picture for the Swift–Hohenberg equation in a finite domain, with branches of localised solutions emerging from the uniform branch at $\mu \approx -0.07$ and turning around in a succession of fold bifurcations to form two intertwined snakes of localised structures, one of site-centered and one of bond-centered solutions, before reconnecting to the uniform branch at $\mu \approx -0.98$. For N even, as is the case in figure 1, these solutions lie in $\mathrm{Fix}(\rho\tau)$ and $\mathrm{Fix}(\rho)$ respectively; this is shown clearly in figure 2.

Again, just as in the continuum Swift–Hohenberg equation, the two snaking branches are connected by 'ladders' of asymmetric structures: the ladders comprise solutions with no symmetry at all that are always unstable. These branches bifurcate subcritically from the main snake, at locations near to the fold bifurcations making up the main body of the snake (not shown in figure 1). Solution profiles at the lowest (in terms of L^2 norm) six right-hand saddle nodes are shown in figure 2. The regions of the (μ, C) plane in which 1-cell, 2-cell and 3-cell states exist are shown in figure 3.

2.5. Neumann boundary conditions

With PBC the bifurcation structure of the discrete model (3) exactly parallels that of the continuous bistable Swift-Hohenberg equation. When we switch to NBC one of the snaking branches persists but the other fragments into a series of isolas (closed curves of equilibria that no longer connect up into a snake) and 'bubbles' (curves of equilibria that begin and end in bifurcations from the persistent snaking curve). In figure 1 the persistent snaking branch is indicated in black, isolas are indicated by the red curves and the bubbles are shown in blue. For N even, the persistent snaking curve consists of bond-centred states with symmetry $\mathrm{Fix}(\rho)$. The two halves of the pitchfork bifurcation where the bond-centred states bifurcate from

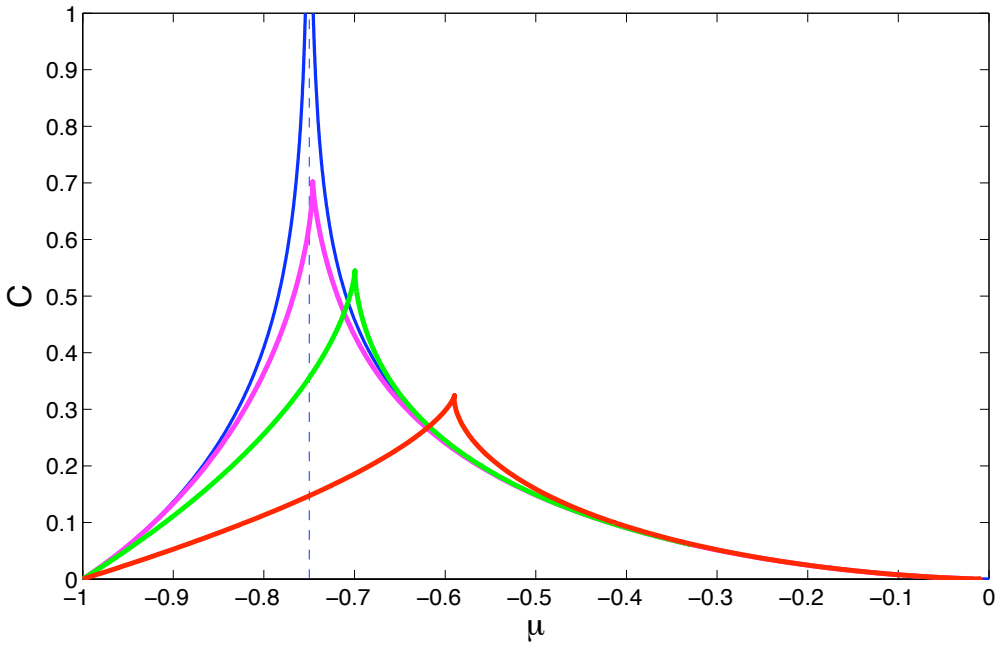

Figure 3: Regions of existence of localised states in the (μ, C) plane: 1-cell localised state (red, peak at $C \approx 0.33$), 2-cell (green, peak at $C \approx 0.55$) and 3-cell (magenta, peak at $C \approx 0.7$). The front solution is indicated by the blue curves which extend up to $C = 1$: on an infinite lattice the edges of the snaking region asymptote to these curves as the width of the localised state increases. The vertical dashed line is the Maxwell point $\mu = -3/4$ for reference. Results obtained for $N = 100$.

the uniform state are no longer related by symmetry: in figure 1(b) we show the branch corresponding to states that are localised in the centre of the lattice rather than at the edges of the lattice.

The snaking curve of site-centred states in figure 1(a) breaks up in figure 1(b) into isolas and bubbles which do not directly interact. In figure 1(b) the lowest isola approaches the bifurcation point where the bond-centred branch connects to the uniform branch but does not bifurcate from either. As the L_2 norm increases, isolas alternate with bubbles which do bifurcate from the bond-centred snaking branch. The bubbles bifurcate from points close to where the 'ladders' bifurcate in figure 1(a) and lack symmetry: in fact they comprise states which evolve smoothly from the exactly bond-centred state on the snaking curve and become very close to the subspace $\mathrm{Fix}(\rho\tau)$ before moving back towards $\mathrm{Fix}(\rho)$ and reconnecting with the snaking branch further up. Moreover there are, properly speaking, four copies of each isola and bubble branch of site-centred asymmetric localised states, related by the symmetries κ and ρ.

This behaviour mimics what has been observed for the Swift–Hohenberg equation with non-periodic boundary conditions [3, 13, 15]. It is important to note however, that in contrast with these investigations, the domain size cannot be used as a continuously varying parameter in the present context. In fact, we anticipate that increasing N by unity reverses the roles of the bond-centred and site-centred solutions when the boundary conditions are left unchanged. For example, with NBC as we consider here, when N is odd we expect the site-centred snaking curve to persist and the bond-centred one to fragment into isolas and bubbles in a manner similar to that shown in figure 1.

3. Two-dimensional lattices

In two dimensions our interpretation of (2) must be modified since there are additional possibilities for the coupling terms. On the square lattice $\mathbb{Z}^2$ there are two natural nearest-neighbour difference operators:

$$\Delta^{+} u_{nm} \equiv u_{n+1,m} + u_{n-1,m} + u_{n,m+1} + u_{n,m-1} - 4u_{nm}, \tag{10}$$

$$\Delta^{\times} u_{nm} \equiv u_{n+1,m+1} + u_{n-1,m-1} + u_{n-1,m+1} + u_{n+1,m-1} - 4u_{nm}. \tag{11}$$

This leads to the following 2D generalization of (3)

$$\dot{u}_{nm} = C^{+}\Delta^{+}u_{nm} + C^{\times}\Delta^{\times}u_{nm} + \mu u_{nm} + 2u_{nm}^{3} - u_{nm}^{5}, \tag{12}$$

where there are now two coupling parameters C^{+} and $C^{\times}$, the coefficients of nearest-neighbor (NN) and next-nearest-neighbor (NNN) coupling. As in the 1D case, (12) is variational. For this equation our primary interest is in establishing that even with PBC there are isolas containing stable localised states. Therefore, we confine our presentation to localised solutions that are far from the lower and upper ends of the snake where reconnection to the uniform state occurs in a finite domain. To further simplify the discussion we set $C^{\times} = 0$ for the remainder of this Letter. Clearly it is of interest to investigate how the snaking structure evolves with $C^{\times}$ nonzero, and we will return to this and other issues in subsequent work.

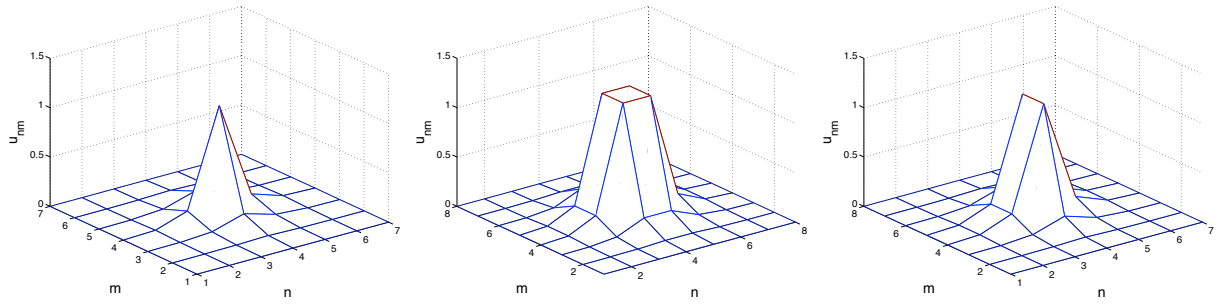

Figure 4: Three typical localised solutions to (12) with $C^{+} = 0.1$, $C^{\times} = 0$ and $\mu = -0.6$. The three solutions are respectively site-centred, bond-centred and hybrid.

The bifurcation structure of localised solutions in 2D is made complicated by the existence of at least three snaking curves: a localised state can be site-centred, bond-centred or a hybrid of the two, being site-centred in one lattice direction and bond-centred in the other (for a more complete discussion see [6]). Examples of each of these types of solutions are shown in figure 4. For simplicity we will now focus on bond-centred states and follow the evolution of snaking curves of such states. Figure 5 shows the evolution of bond-centred localised states along the continuous snaking curve shown in figure 6(b).

3.1. Bifurcation structure of localised states

It is not at all clear theoretically how the well-established theory for homoclinic snaking in 1D extends to 2D since there does not appear to be an analogous paradigm to the spatial dynamics approach. However, numerical computations show that the bifurcation diagram for localised states contains qualitative similarities (see Figure 6). We remark that to generate this figure our computations were carried out using AUTO on a 20×20 grid. To accelerate the computation we simulated only a quarter of the domain, using appropriate 'reflecting' boundary conditions to ensure that the new states generated were bond centred. This imposed symmetry implies that bifurcations to asymmetric 'ladder' states could not be detected. Other computations indicate that such bifurcations exist, and we will discuss the existence of asymmetric states elsewhere.

The states shown in figure 5 lie on the snaking curve shown in figure 6(b) in which the bifurcation parameter μ is plotted on the vertical axis and the solution measure M^2 on the horizontal axis. M is a scaled version of the L_2 norm defined as:

$$M = \left(\frac{\sum_{n,m} u_{nm}^{2}}{1 + \sqrt{1+\mu}} \right)^{1/2}.$$

Use of the solution measure M confers the advantage that at low coupling strengths it measures the (near-integer) number of cells that are 'active' in the localised state. Figure 6(a) indicates that 'high peaks' (e.g. the saddle-nodes labelled (a), (b), (c), (e) and (f) at which the value of μ is markedly less negative than

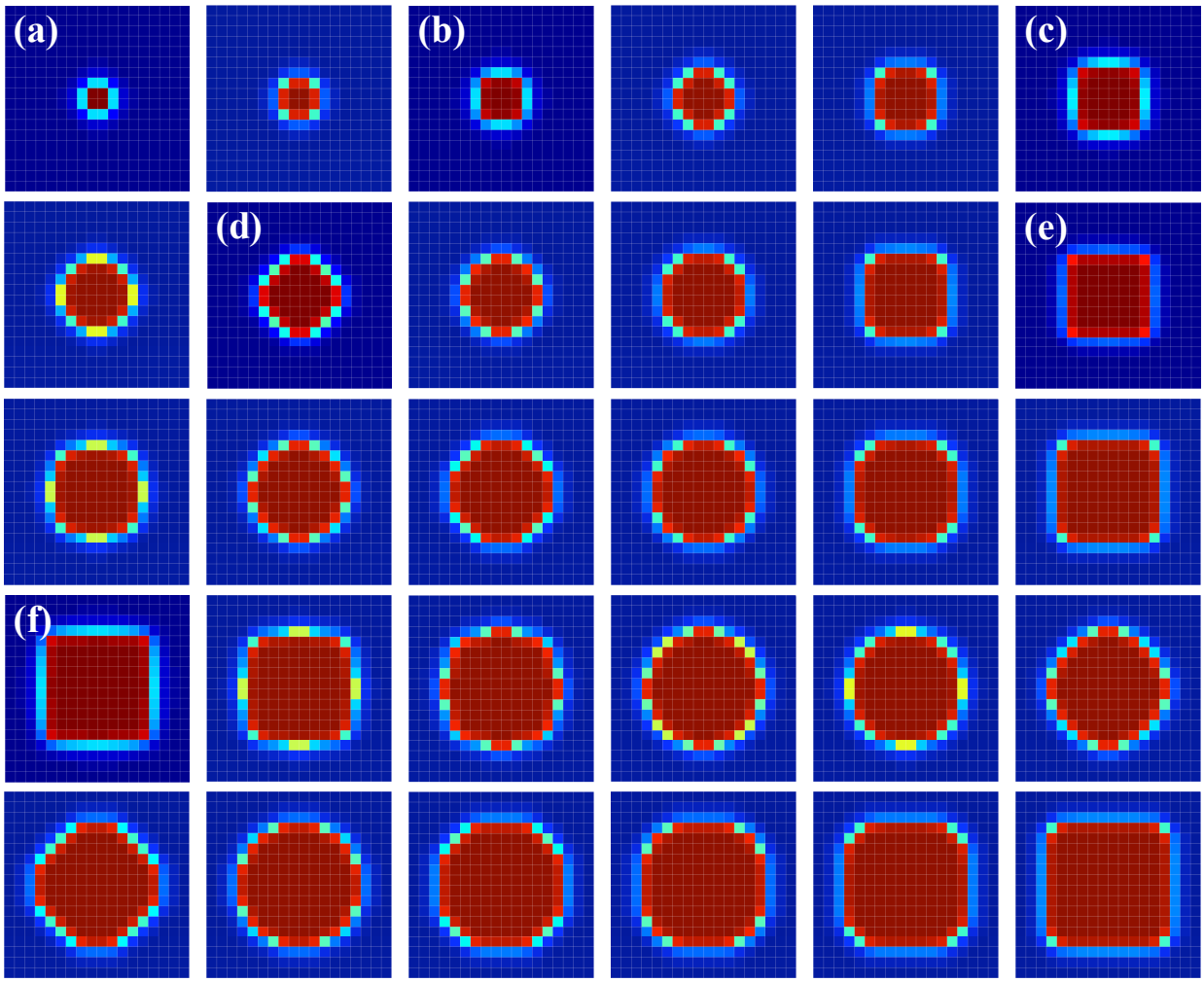

Figure 5: The first 30 bond-centred localised states encountered at saddle-node bifurcation points corresponding to local maxima of μ, moving along the snaking curve with M increasing, for fixed $C^+ = 0.2$. Labels (a) - (f) correspond to the labelled saddle-node bifurcations on the snake indicated in figure 6(b).

at most saddle-nodes) are closely aligned with even integer values of M. These labels correspond to the labelled localised states in figure 5 that are in the form of complete $2k \times 2k$ square arrays of active cells.

The evolution of bond-centred localised states as we move up the snaking curve is shown in figure 5. Starting from 5(a) in which four cells are close to u_+ and the rest are near zero, new u_+ cells are added to the solution profile starting in the centre of the faces, and then progressing outwards towards the corners until the profile is square, at which point the sequence repeats itself. Numerical continuation suggests that it is possible to proceed arbitrarily far up the snaking curve in this manner as long as the coupling coefficient is sufficiently small. There are similar snaking curves of site-centred and hybrid localised states which for brevity, and because it is not central to our discussion of isolas, we will not discuss here.

3.2. Snaking limits

The horizontal lines in each part of figure 6 indicate the locations of saddle-node bifurcations far up the 1D snake for two values of the coupling coefficient: $C = C^+ + 2C^\times$ (red) and $C = 2C^+ + C^\times$ (blue). These values are determined from the part of the blue curve in figure 3 which lies in $\mu > -0.75$.

At small coupling strengths it is clear numerically in figure 7(a) that, as M^2 increases and we move far up the snaking curve, the width of the snaking region is given overall by $C = C^+$ since the existence of square $2k \times 2k$ arrays of localised states is determined by the existence of stationary fronts aligned with a lattice direction. This is easy to see from the lattice equations 12) by removing the dependence on the second coordinate m, i.e. setting $u_{nm} = u_n$ we recover (3) with $C = C^+ + 2C^\times$. All other saddle-node bifurcations involve localised states which are not complete squares and therefore involve stationary diagonal fronts between u_+ and zero. Substituting the ansatz $u_{nm} = u_\ell$ where $\ell = n + m$ into (12) we obtain

$$\dot{u}_\ell = 2C^+(u_{\ell+1} + u_{\ell-1} - 2u_\ell) + C^\times(u_{\ell+2} + u_{\ell-2} - 2u_\ell) + \mu u_\ell + 2u_\ell^3 - u_\ell^5. \tag{13}$$

Hence, in the case $C^\times = 0$ this reduces exactly to (3) with $C = 2C^+$. When $C^\times \neq 0$ and the coupling coefficients are small (and hence the front is sharp compared to the lattice spacing) we anticipate that $u_{\ell+2} \approx u_{\ell+1} \approx u_+$ on one side of the front and $u_{\ell-2} \approx u_{\ell-1} \approx 0$ on the other and so (13) can be well approximated by (3) setting $C = C^+ + 2C^\times$.

Figure 6(d) shows the bond-centred snake with $C^+ = 0.1$ and $C^\times = 0.05$. Qualitatively there is little difference between this and parts (a) and (b). We observe two distinct scales in the bifurcation diagram, with the widths of turns on the snake corresponding roughly to those in the 1D model with $C = C^+ + 2C^\times$ or $C = 2C^+ + C^\times$. We anticipate that for $C^\times$ small compared with C^+ there will be no significant differences from the $C^\times = 0$ case, but numerical continuation suggests that larger $C^\times$ can alter the snaking curve significantly, especially when $C^\times > C^+$. We should also note that with two independent coupling parameters there is no equivalent to the staggering transformation presented for the 1D model.

3.3. Switchbacks

As the coupling strength C^+ increases the snaking curves quantitatively depart from the 1D case due to the existence of regions in the bifurcation diagram where the snaking curve turns back on itself and the L_2 norm (or, equivalently, M) of the localised state descreases for a number of twists before turning back again and continuing to snake upwards. We refer to such an episode as a 'switchback'. Examples of switchbacks are shown in figure 7. In part (a) of figure 6 switchbacks are observed to begin only at $M^2 \approx 64$, 100 and 144. In (b) an additional switchback appears at $M^2 \approx 36$. In (c) almost all the twists in the switchbacks have disappeared, although the bifurcation curves near $M^2 = 64$, 100 and 144 show clear similarities.

We find that the appearance and disappearance of switchbacks as the coupling strength C^+ is varied can be explained by collisions between solution curves in the bifurcation diagram. When C^+ is small it is important to note that there are many localised solutions to (12) possessing square symmetry which do not appear on the snaking curve, e.g. as shown in figure 6(a). These additional localised states exist on isolas in the bifurcation diagram. As C^+ is increased these isolas collide with the snaking branch and form a switchback. Assuming, as is reasonable at low coupling strength, that the isola contained a stable solution, the snaking curve will now contain (at least) one extra stable solution, by which we mean a localised state now present, but not present on the snake at lower C^+. As C^+ is increased still further the snake narrows. Intriguingly, and unexpectedly, the switchback may detach itself from the snake as C^+ is increased further, re-forming a disconnected isola. Figure 8 illustrates these events with a sequence of bifurcation diagrams in the (μ, L_2) plane. The processes of attachment and detachment are facilitated by cusp singularities in which pairs of saddle-nodes on the snake collide and disappear as the coupling strength increases. Figure 9 shows the cusp bifurcations in the (μ, C^+) plane corresponding to the attachment and detachment of the isola near $M^2 = 36$ shown in figure 7(a) and figure 8.

In summary these isolas provide a mechanism by which additional turns can be added to the snake, and they explain the unintuitive switchback episodes of the snaking curve as the localised states increase in size. This process of isola attachment and detachment typically occurs over a remarkably small range of C^+, indicated by the vertical scales in figure 9. At larger L_2 norms the complete bifurcation diagram in the (μ, C^+) plane is complicated since many isolas attach and detach from the snake at nearby values of C^+.

4. Summary

In this Letter we have discussed the bifurcation structure of a model lattice equation, the discrete Allen-Cahn equation with cubic and quintic nonlinearities, in one and two dimensions. This equation is of interest in its own right as a model for spatially discrete pattern formation as well as being closely related to coupled nonlinear Schrödinger equations which have received substantial recent attention in nonlinear optics. A subcritical instability of the trivial state, and the resulting bistability, leads to the creation of localised states which are stable over an open interval of the parameter μ, stabilized by being pinned to the lattice. As remarked on by previous authors, these localised states arrange themselves into homoclinic snaking curves. In a finite domain we demonstrated the existence of a maximum coupling strength above which there is no modulational secondary instability which would allow creation of localised states: in systems with a sufficiently large coupling strength localised states do not appear.

In 1D we showed that breaking discrete translational symmetry, for example by using Neumann boundary conditions, allows one of the snakes to persist, but causes the other to fragment into a sequence of isolas and bubbles ('S'–shaped curves bifurcating from the persistent snake). This contrasts with the situation in 2D where isolas exist even when discrete translational symmetry is not broken. These isolas attach and detach themselves from the primary snaking curve as the linear coupling strength is varied, creating kinks in the snaking curve, where the solution norm decreases along a part of the curve before beginning to increase again, that we refer to as 'switchbacks'.

Numerical investigations suggest quantitative relations between the widths of the snaking curves in 1D and 2D. For wide localised states in 2D the values of μ that limit the region over which localised states exist correspond to the limiting values for fronts aligned with lattice directions or on the diagonal. This is the natural interpretation and agrees with the observations and computations by Lloyd et al. [19] for localised patches of hexagons in the 2D Swift–Hohenberg equation. This correspondence between 1D and 2D is asymptotically exact in the limit of small coupling coefficients: higher-order corrections arise at non-zero coupling and from the corners of the wide localised state where the fronts meet.

Our results are closely related to the work of Carretero-Gonzàles and Chong et al. [6, 8] on the discrete nonlinear Schrödinger equation with cubic and quintic nonlinearities. They discussed the time-independent Allen-Cahn equation from a spatial dynamics viewpoint, explaining the one-dimensional snaking curve as arising from intersections of the stable and unstable manifolds of a hyperbolic fixed point in a two-dimensional map. They also explored a variational approach, minimizing an effective Lagrangian to give approximate localised states in one and two dimensions.

Our work considers additional mechanisms that complicate the usual snaking picture by causing isolas to appear: these include the effect of boundary conditions in 1D and exploring larger localised states, higher up the snaking curve in 2D where new effects, including the switchbacks, arise.

References

[1] N. Akhmediev and A. Ankiewicz (eds) 2005 *Dissipative Solitons*. Lect. Notes in Physics **661**. Springer, Berlin.

[2] F. Antoneli, A.P.S. Dias, M. Golubitsky & Y. Wang 2005 Patterns of synchrony in lattice dynamical systems. *Nonlinearity* **18**, 2193–2209

[3] A. Bergeon, J. Burke, E. Knobloch & I. Mercader 2008 Eckhaus instability and homoclinic snaking. *Phys. Rev.* E **78**, 046201

[4] J. Burke and E. Knobloch 2006 Localized states in the generalized Swift–Hohenberg equation. *Phys. Rev.* E **73**, 056211

[5] J. Burke and E. Knobloch 2007 Snakes and ladders: localized states in the Swift–Hohenberg equation. *Phys. Lett.* A **360**, 681–688

[6] R. Carretero-Gonzàlez, J.D. Talley, C. Chong and B.A. Malomed 2006 Multistable solitons in the cubic-quintic discrete nonlinear Schrödinger equation. *Physica* D **216** 77–89

[7] S.J. Chapman and G. Kozyreff 2009 Exponential asymptotics of localised patterns and snaking bifurcation diagrams. *Physica* D **238**, 319–354

[8] C. Chong, R. Carretero-González, B.A. Malomed and P.G. Kevrekedis 2009 Multistable solitons in higher-dimensional cubic-quintic nonlinear Schrödinger lattices. *Physica* D **238**, 126–136

[9] S.-N. Chow, J. Mallet-Paret & E.S. Van Vleck 1996 Pattern formation and spatial chaos in spatially discrete evolution equations. *Random & Computational Dynamics* **4**, 109–178

[10] J.R. Collier, N.A.M. Monk, P.K. Maini & J.H. Lewis 1996 Pattern formation by lateral inhibition with feedback: a mathematical model of Delta–Notch intercellular signalling. *J. Theor. Biol.* **183**, 429–446

[11] P. Coullet, C. Riera and C. Tresser 2000 Stable static localized structures in one dimension. *Phys. Rev. Lett.* **84**, 3069–3072
[12] M.C. Cross & P.C. Hohenberg 1993 Pattern formation outside of equilibrium. *Rev. Mod. Phys.* **65** 851–1112
[13] J.H.P. Dawes 2009 Modulated and localised states in a finite domain. *SIAM J. Appl. Dyn. Syst.* **8**, 909–930
[14] E. J. Doedel, A.R Champneys, T. Fairgrieve, Y. Kuznetsov, B. Oldeman, R. Paffenroth, B. Sandstede, X. Wang and C. Zhang 2007 AUTO-07p: continuation and bifurcation software for ordinary differential equations. Available to download from `http://indy.cs.concordia.ca/auto/`.
[15] S.M. Houghton and E. Knobloch 2009 Homoclinic snaking in bounded domains. *Phys. Rev.* E **80**, 026210
[16] R.B. Hoyle 2006 *Pattern Formation: An Introduction to Methods*. CUP, Cambridge, UK.
[17] G. Iooss and M.-C. Pérouème 1993 Periodic homoclinic solutions in reversible 1 : 1 resonance vector fields. *J. Diff. Eq.* **102**, 62–88
[18] G. Kozyreff and S.J. Chapman 2006 Asymptotics of large bound states of localized structures. *Phys. Rev. Lett.* **97**, 044502
[19] D.J.B. Lloyd, B. Sandstede, D. Avitabile and A.R. Champneys 2008 Localized hexagon patterns of the planar Swift–Hohenberg equation. *SIAM J. Appl. Dyn. Syst.* **7**, 1049
[20] M.R. Owen, J.A. Sherratt & H.J. Wearing 2000 Lateral induction by juxtacrine signalling is a new mechanism for pattern formation. *Developmental Biology* **217**, 54–61
[21] L.M. Pismen 2006 *Patterns and Interfaces in Dissipative Dynamics*. Springer, Berlin.
[22] J. Swift & P.C. Hohenberg 1977 Hydrodynamic fluctuations at the convective instability. *Phys. Rev.* A **15**, 319–328
[23] Y. Wang & M. Golubitsky 2005 Two-color patterns of synchrony in lattice dynamical systems. *Nonlinearity* **18**, 631–657
[24] S.D. Webb & M.R. Owen, 2004 Oscillations and patterns in spatially discrete models for developmental ligand-receptor interactions. *J. Math. Biol.* **48**, 444–476
[25] P.D. Woods & A.R. Champneys 1999 Heteroclinic tangles and homoclinic snaking in the unfolding of a degenerate reversible Hamiltonian–Hopf bifurcation. *Physica* D **129**, 147–170
[26] A.V. Yulin, A.R. Champneys & D.V. Skryabin 2008 Discrete cavity solitons due to saturable nonlinearity. *Phys. Rev.* A **78**, 011804
[27] A.V. Yulin & A.R. Champneys 2009 Discrete snaking: multiple cavity solitons in saturable media. Preprint.

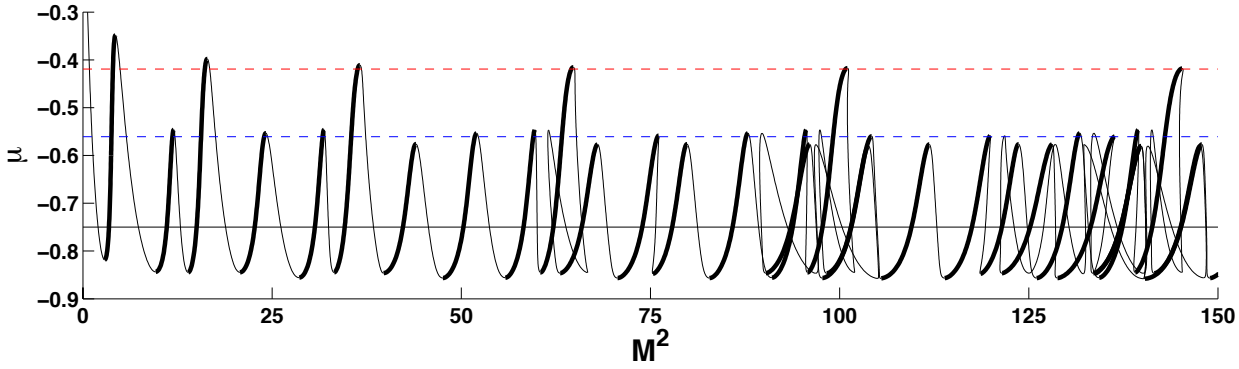

(a)

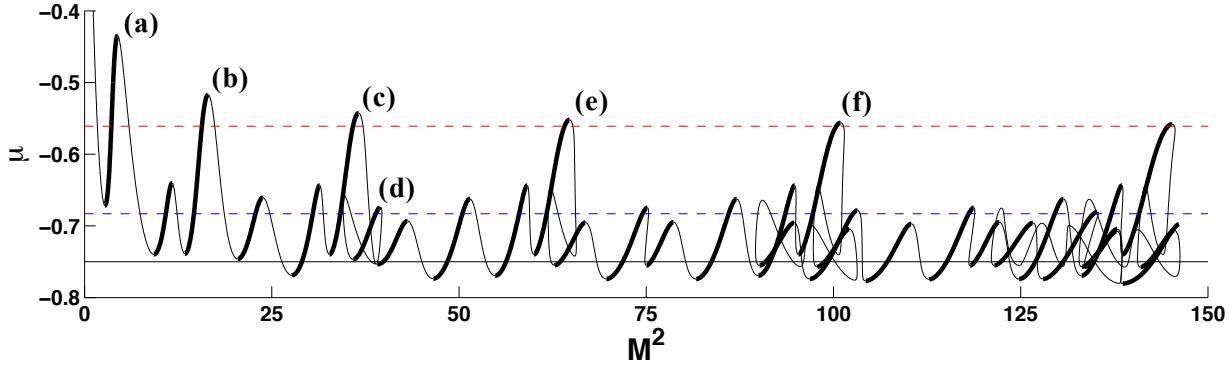

(b)

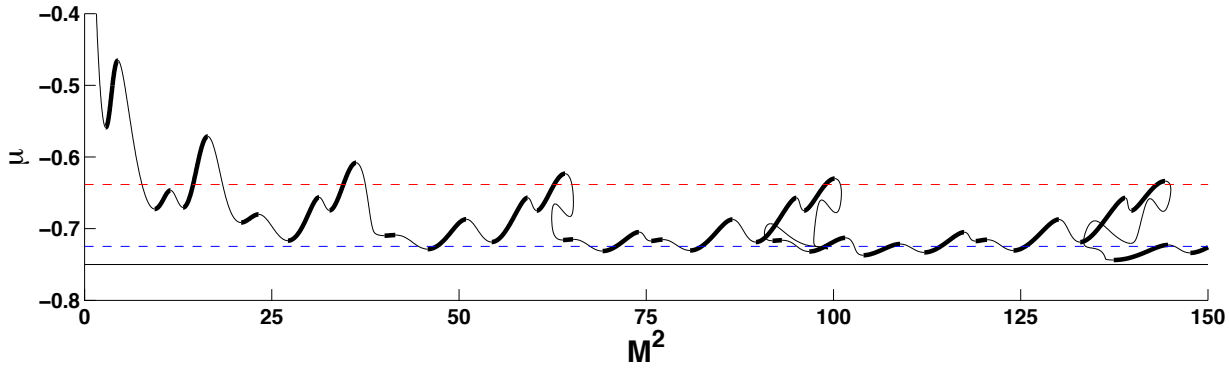

(c)

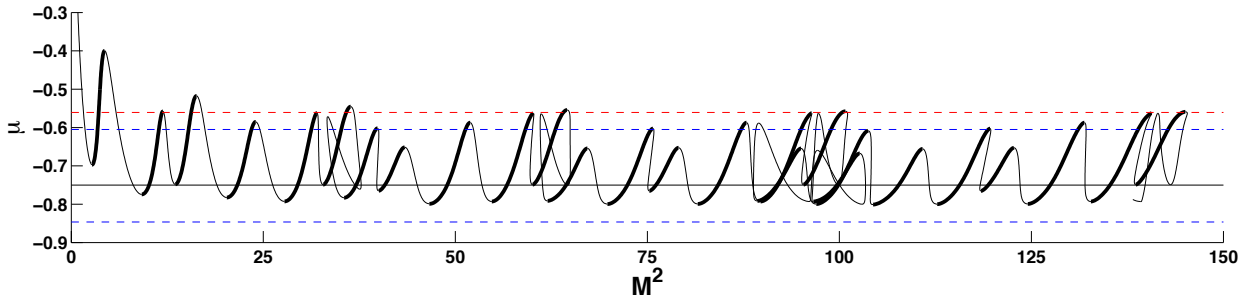

(d)

Figure 6: Snaking of bond-centred solutions to (12) with (a) $C^+ = 0.1$, (b) $C^+ = 0.2$, (c) $C^+ = 0.3$ (in all cases $C^\times = 0$ and (d) $C^+ = 0.1$, $C^\times = 0.05$. Note the switchbacks in (b) occur near $M^2 = 36$, 64, 100 and 144, see also figure 7. Solid black lines indicate the Maxwell point $\mu = -0.75$. Red horizontal dashed lines at (a) $\mu \approx -0.41925$, (b) $\mu \approx -0.56076$, (c) $\mu \approx -0.63832$ and (d) $\mu \approx -0.56076$ indicate the asymptotic location of saddle-node bifurcations on the 1D snake with coupling strength $C = C^+ + 2C^\times$, far up the 1D snake. Blue horizontal dashed lines at (a) $\mu \approx -0.56076$, (b) $\mu \approx -0.68309$, (c) $\mu \approx -0.72479$ and (d) $\mu \approx -0.60495$ indicate the asymptotic location of saddle-node bifurcations on the 1D snake with coupling strength $C = 2C^+ + C^\times$. Thin and thick lines indicate unstable and stable solutions, respectively. Labels (a) - (f) in part (b) correspond to the solutions labelled in figure 5.

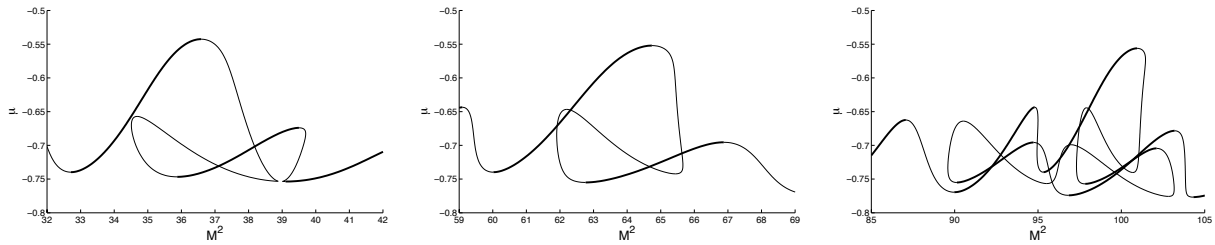

(a) (b) (c)

Figure 7: (a) Enlargement of figure 6(b) at the first switchback, near $M^2 = 36$; (b) a second switchback near $M^2 = 64$; (c) a much more complicated switchback near $M^2 = 100$.

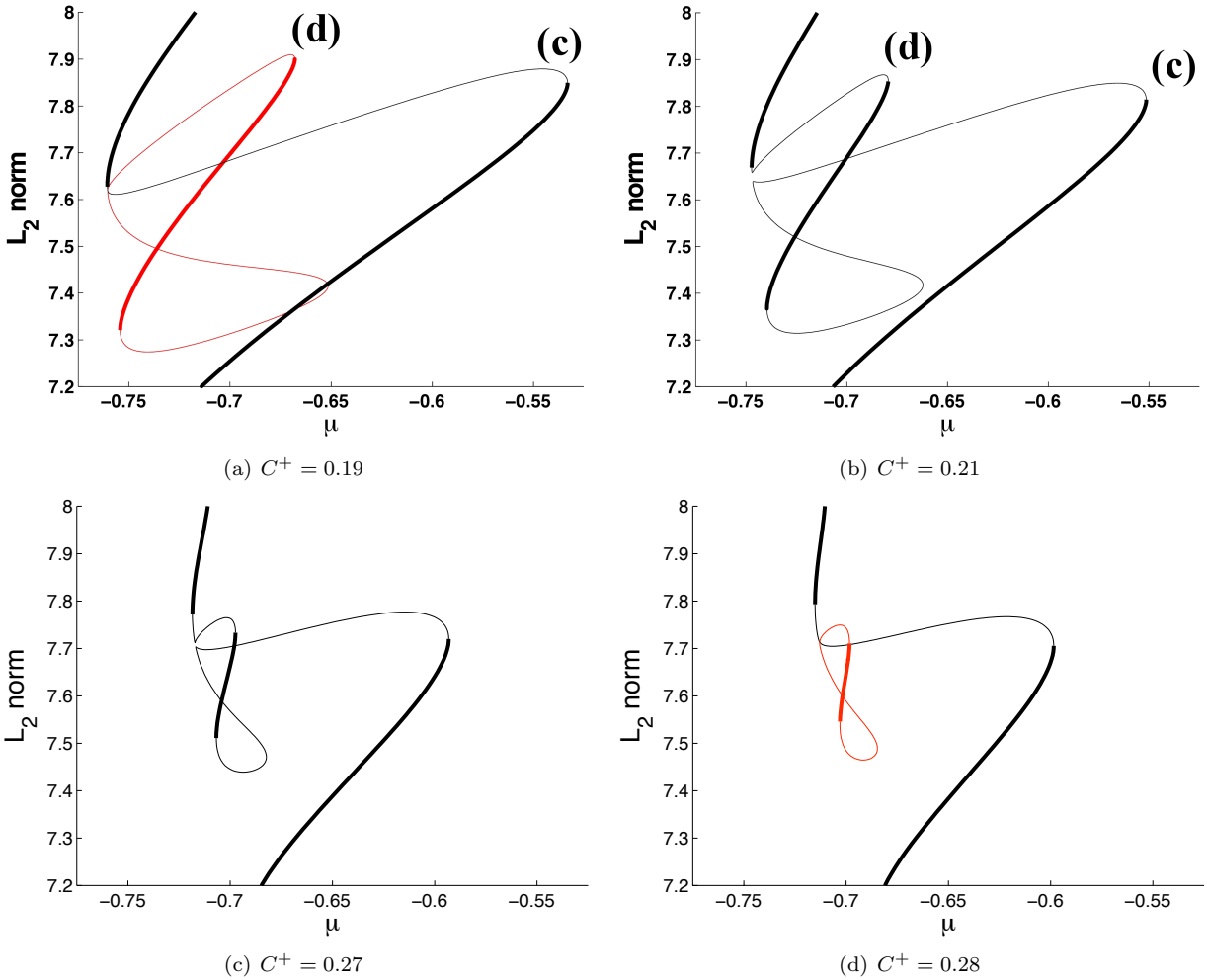

(a) $C^+ = 0.19$ (b) $C^+ = 0.21$

(c) $C^+ = 0.27$ (d) $C^+ = 0.28$

Figure 8: (a) The snaking curve (black) and an unconnected isola (red) at $C^+ = 0.19$, (b) topology change in the snaking curve as we increase the coupling strength, creating a switchback, (c) narrowing of the snaking curve as coupling strength is increased further, (d) eventual detachment of the switchback to form another isola. The labels **(c)** and **(d)** in parts (a) and (b) correspond to the saddle-nodes labelled in figure 6(b) and the solution plots shown, respectively, in figures 5(c) and 5(d).

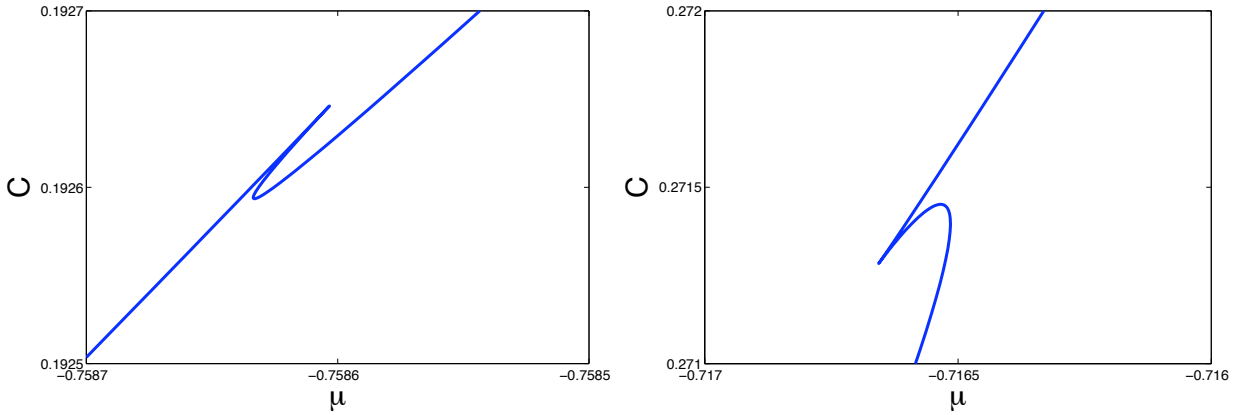

Figure 9: The process of isola attachment and detachment in the (μ, C) plane by following limit points: on the left an isola attaches itself to the snake as C^+ is increased, briefly creating a situation with three limit points, two of which disappear in a cusp singularity [corresponding to Fig. 8(a)–(b)], and on the right the same process in reverse, as an isola detaches at a higher value of C^+ [corresponding to Fig. 8(c)–(d)].